Accepted Manuscript

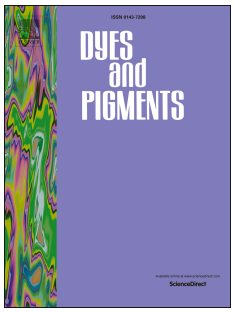

Amplified singlet oxygen generation in metallated-porphyrin doped conjugated polymer nanoparticles

Ramiro M. Spada, Lorena P. Macor, Laura I. Hernández, Rodrigo A. Ponzio, Luis E. Ibarra, Carolina Lorente, Carlos A. Chesta, Rodrigo E. Palacios

PII: S0143-7208(17)31668-6

DOI: 10.1016/j.dyepig.2017.09.044

Reference: DYPI 6269

To appear in: *Dyes and Pigments*

Received Date: 3 August 2017

Accepted Date: 17 September 2017

Please cite this article as: Spada RM, Macor LP, Hernández LI, Ponzio RA, Ibarra LE, Lorente C, Chesta CA, Palacios RE, Amplified singlet oxygen generation in metallated-porphyrin doped conjugated polymer nanoparticles, *Dyes and Pigments* (2017), doi: 10.1016/j.dyepig.2017.09.044.

Amplified singlet oxygen generation in metallated-porphyrin doped conjugated polymer nanoparticles.

Ramiro M. Spada [a,1], Lorena P. Macor [a,1], Laura I. Hernández [a,1], Rodrigo A. Ponzio [a,b], Luis E. Ibarra [c] , Carolina Lorente [d], Carlos A. Chesta [a,*] and Rodrigo E. Palacios [a,*]

[a] *Universidad Nacional de Río Cuarto y CONICET, Dto. Química, Facultad de Ciencias Exactas Fisicoquímicas y Naturales, Río Cuarto (5800), Córdoba, Argentina.* Instituto de Investigaciones en Tecnologías Energéticas y Materiales Avanzados (IITEMA), Argentina.

[b] *Universidad Nacional de Río Cuarto, Dto. Física, Facultad de Ciencias Exactas Fisicoquímicas y Naturales, Río Cuarto (5800), Córdoba, Argentina.*

[c] *Universidad Nacional de Río Cuarto y CONICET, Dto. Biología Molecular, Facultad de Ciencias Exactas Fisicoquímicas y Naturales, Río Cuarto (5800), Córdoba, Argentina.*

[d] *Universidad Nacional de La Plata y CONICET, Instituto de Investigaciones Fisicoquímicas Teóricas y Aplicadas (INIFTA), Departamento de Química, Facultad de Ciencias Exactas, CCT La Plata CONICET, La Plata (1900), Buenos Aires, Argentina.*

Abstract

We report on the mechanism and efficiencies of singlet oxygen $O_2(^1\Delta_g)$ generation of nanoparticles (NP) of the conjugated polymer (CP) poly(9,9-dioctylfluorene-alt-benzothiadiazole) (F8BT) doped with platinum octaethylporphyrin (PtOEP) suspended in water. A detailed study of the photophysics of these NP, using stationary and time-resolved absorption and emission techniques, indicates that $O_2(^1\Delta_g)$ is generated by the triplet excited state of F8BT and not by that of PtOEP, as previously observed for other porphyrin doped CP NP. $O_2(^1\Delta_g)$ quantum yields (Φ_Δ) were measured by quantifying the characteristic phosphorescence of $O_2(^1\Delta_g)$ in the NIR region (~ 1268 nm). It was found that incorporation of relatively small amounts of PtOEP to F8BT NP results in a significant increase of Φ_Δ. NP containing 10% PtOEP (w/w) show a $\Phi_\Delta \sim 0.24$, which is 3 times larger than that observed for undoped F8BT NP, and larger than the reported for most water-soluble porphyrins. Φ_Δ were also calculated from the oxidation rates (v_0) of 3-10-(2-carboxyethyl) anthracene (ADPA), a well-known chemical $O_2(^1\Delta_g)$ trap. Unexpectedly, this method was found to significantly overestimate the Φ_Δ values due to the adsorption of ADPA on the surface of NP. The ADPA / NP adsorption process was characterized using a simple adsorption model yielding an (average) equilibrium constant of $\sim 8 \times 10^3$ M^{-1} and an (average) number of NP-binding sites of ~14000. These

* Corresponding author. Tel.: +54-9358-423-9820; fax: +54-358-467-6000; e-mail: rpalacios@exa.unrc.edu.ar

[1] These authors contributed equally to this work

results necessarily caution about the use of ADPA as a probe to evaluate Φ_Δ in these NP systems. In addition, the interaction of F8BT NP with other anionic, cationic and zwitterionic dyes (dissolved in water) was studied. It was found that even at nano-molar concentrations all the dyes efficiently adsorb on the NP surface. This general and simple self-assembly strategy can be used to prepare superficially-dye-doped CP NP with potentially interesting technological applications.

Keywords.

conjugated polymer nanoparticles; metallated porphyrin; photosensitization; singlet oxygen quantum yield; dye adsorption;

1. Introduction

Conjugated polymers (CP) are formed by monomers linked together by alternating single and double (or triple) bonds along the backbone chain. This extended conjugation structure gives these materials unique properties that allow their application in organic-electronic devices such as solar cells [1,2], organic light emitting diodes (OLED) [3], fluorescence-based sensors [4–6], etc. Nanoparticles of conjugated polymers (CP NP) show small size (<100 nm), extraordinarily large excitation cross-sections, high brightness, photochemical stability and several other appealing photophysical properties that make them useful in the development of fluorescence based chemical, physical and biological nano-sensors [7–16]. Comprehensive reviews on CP NP characteristics and applications have been recently published [17–20]. In particular, the exceptional light harvesting and energy transfer properties of CP NP have been exploited in the development of novel $O_2(^1\Delta_g)$ photosensitizer materials used for anticancer and antibacterial treatments [18,21–31]. In these particles the polymer matrix acts as efficient antenna by collecting visible (or NIR) photons and efficiently transferring excitation energy to photosensitizing dopant molecules (PS) amplifying their intrinsic $O_2(^1\Delta_g)$ generation efficiencies [17]. However, the search for optimized CP NP for photodynamic (PDT) and photothermal cancer therapy remains very active. Recently, Wu *et al*. [25,26] reported the synthesis and characterization of CP NP made of poly(9,9-dioctylfluorene-alt-benzothiadiazole) (F8BT) doped with tetraphenylporphyrin free base (TPP) as PS (F8BT-TPP NP). According to these studies, upon excitation of F8BT-TTP NP the CP can efficiently transfer (singlet) excitation energy to TPP, which efficiently generates the porphyrin triplet excited state (^{3}TPP*). In turn, ^{3}TPP* can be intercepted by molecular oxygen to give $O_2(^1\Delta_g)$. Thus, these TPP doped CP NP were shown to photosensitize the formation of $O_2(^1\Delta_g)$ and were successfully used for *in vitro* and *in vivo* PDT experiments. The reported Φ_Δ (~0.3-0.5) for these particles was estimated using an indirect method based on the consumption of a water soluble anthracene derivative that reacts efficiently with $O_2(^1\Delta_g)$ [25,26].

We report herein the synthesis and an exhaustive photophysical/photochemical characterization of F8BT NP doped with platinum octaethylporphyrin (PtOEP). As in the case of TPP, PtOEP can photosensitize $O_2(^1\Delta_g)$ formation quite efficiently [32] and therefore, a significant increase in Φ_Δ was expected upon PtOEP doping. The Φ_Δ of undoped and PtOEP doped F8BT NP suspended in water was measured using direct

(singlet oxygen phosphorescence detection) and indirect (comparative rates for chemical traps oxidation) methods. Indirect methods to asses $O_2(^1\Delta_g)$ production, which are based on the chemical transformation of an organic substrate upon reaction with $O_2(^1\Delta_g)$, are widely used because they are simple and inexpensive [33–39]. However, we prove here that indirect methods can significantly overestimate Φ_Δ due to the adsorption of the $O_2(^1\Delta_g)$ trap (substrate) on the NP´s surface. Thus, our results caution about the use of this method for measuring Φ_Δ in these systems. However, this combined organic substrate adsorption and enhanced photosensitized oxidation capacity of these PtOEP doped F8BT NP bodes well for their use in PDT and in organic water pollutants photoremediation strategies. Additionally, we demonstrate that the efficient and spontaneous adsorption of other organic molecules containing ionizable groups (anionic, cationic and zwitterionic organic dyes) to the surface of F8BT NP in water at nanomolar concentrations can be used as a simple and general strategy to achieve superficial dye doping of these conjugated polymer nanoparticles.

2. Experimental

2.1. Materials. 3-10-(2-carboxyethyl)anthracene (ADPA, 99%, Sigma-Aldrich) and 9,10-dimethylanthracene (DMA, 99%, Sigma-Aldrich), furfuryl alcohol (FFA, 98%, Sigma-Aldrich), rhodamine-B (95%, Aldrich), platinum octaethylporphyrin (PtOEP, >95%, Frontier Scientific), poly(9,9-dioctylfluorene-alt-benzothiadiazole) (F8BT, MW=70000 g/mol, PDI=2.4, American Dye Source Inc.), methylene blue (MB, 82%, Aldrich), rose bengal (RB, 95%, Aldrich), rhodamine B (RhB, 95%, Sigma-Aldrich), acetonitrile (MeCN, HPLC grade, Sintorgan), deuterium oxide (D_2O, 99.9%, Sigma-Aldrich), were used as received. Chemical structures of the dyes F8BT, PtOEP, MB and RB are shown in Scheme 1. Tetrahydrofuran (THF, HPLC grade, Cicarelli) was refluxed for 5 hs with potassium hydroxide pellets (KOH, pro-analysis grade, Taurus) and subsequently distilled over freshly activated molecular sieves (4 Å, Aldrich). Double-distill water was further purified by an ELGA PURELAB Classic UV system (~18.2 MΩ/cm) to remove ions, organic and particulate matter (0.2 μM filter). Argon (Ar, 99.998 %, Linde) was used as received.

2.2. Nanoparticle Synthesis. NP were prepared by the re-precipitation method [40–42]. For neat F8BT nanoparticles (F8BT NP), F8BT was dissolved (with the aid of

sonication and mild heating ~ 40° C) in freshly distilled THF to a concentration of ~ 500 mg/L. The solution was filtered with a 0.2 μm pore-size PTFE membrane syringe filter (Iso-Disc, Sigma-Aldrich) to remove any undissolved polymer. The concentration of the filtered solution was recalculated by comparing absorption spectra before and after filtration, and the resulting solution was diluted to a final concentration of 100 mg/L. A small volume (300 μL) of this solution was quickly injected into a vial containing 2.5 mL of either pure water or a low ionic strength buffer solution or acetonitrile under vigorous stirring. Upon contact with water (or acetonitrile) the polymer chains collapse forming nanoparticles containing of one or several chains (nanoaggregates) [42]. PtOEP doped nanoparticles (F8BT-PtOEP NP) were prepared in an analogous manner using THF solutions containing both F8BT (100 mg/L) and PtOEP (10 mg/L). The null solubility of PtOEP in water ensures that the dye is trapped within the polymer matrix (where it is stabilized by van der Waals' interactions) during the formation of the NP. Varying degrees of doping are indicated as F8BT-#PtOEP NP where # is the PtOEP/F8BT % weight ratio.

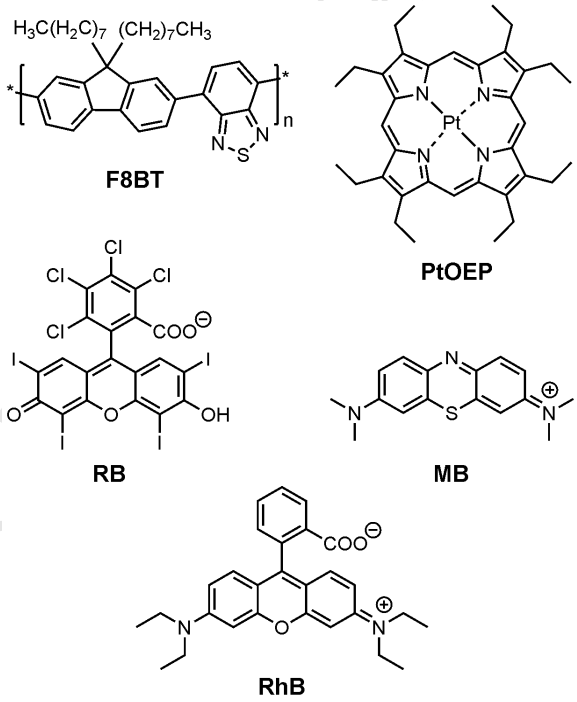

Scheme 1. Molecular structures of F8BT conjugated polymer, PtOEP porphyrin photosensitizer, RB, MB and RhB ionic dyes at neutral pH.

2.3. Steady-state absorption and emission spectroscopy. UV-Vis absorption spectra were recorded on a Diode-Array spectrophotometer (HP 8452A, Agilent Hewlett-Packard) in 1 cm cuvettes at room temperature. Emission spectra were obtained with a

spectrofluorometer (FluoroMax-4, Horiba). Unless other conditions are specified, emission and excitation spectra were acquired from dilute solutions ($Abs_{max} < 0.1$) using the following parameters: 2 nm slits for both the excitation and emission monochromators, 0.1 s integration time per point. Spectra were corrected for the spectral instrument response. The emission spectra were measured in 1 cm cuvettes at room temperature and with excitation at the absorption maximum. Fluorescence quantum yields (Φ_F) were measured with the comparative method using RhB in ethanol at room temperature ($\Phi_F = 0.7$ in ethanol) [43] as the reference.

Steady-state singlet oxygen phosphorescence measurements were carried-out using a NIR PMT Module H10330-45 (Hamamatsu) coupled to a single-photon-counting equipment FL3 TCSPC-SP (Horiba Jobin Yvon) fitted with a Xe (CW 450 W) lamp, excitation (FL-1004 with a 1200 groove per mm, 330 nm blaze grating) and emission (FL-1004 with a 600 groove per mm, 1000 nm blaze grating) monochromators. Absorbance of NP samples and reference (Eosin Y, $\Phi_\Delta = 0.58$ in D_2O) [44] were matched at 487 nm and $O_2(^1\Delta_g)$ phosphorescence was detected at 90° with respect to the excitation beam. Corrected emission spectra obtained with excitation at 487 nm were recorded between 950 and 1400 nm and the total integrated phosphorescence intensities were calculated by integrating the emission band centered at 1268 nm. All experiments were performed in D_2O at room temperature.

2.4. Time-resolved Emission Spectroscopy. Fluorescence lifetimes measurements were performed using the Single Photon Counting (TC-SPC) technique in Edinburgh Analytical Instruments FL- 900 CDT spectrofluorometer equipped with a pulsed light emitting diode (LEDs, PLS450, PicoQuant). The diode used has emission centered at 450 nm (FWHM~ 10 nm) and a typical pulse width of ~ 0.8 ns FWHM.

2.5. Time-resolved Absorption Spectroscopy. Nanosecond laser flash photolysis experiments were performed in air or Ar saturated solutions by exciting at 355 nm (pulse width FWHM ~ 15 ns and energy ~ 2 mJ) and sweeping the absorption spectra between 400 and 640 nm. The instrument has been previously described [45]. Sample absorption at the excitation wavelength was ~ 0.3. Data analysis was carried out using the program ASUFIT, available at http://www.public. asu.edu/laserweb/asufit/asufit.html).

2.6. Single Particle Fluorescence measurements. Nanoparticles suspensions were spin coated on freshly cleaned coverslips to an average surface concentration < 0.1

particle/μm^2 to allow for individual particle identification. The samples were studied in a homemade inverted fluorescence microscope assembled on a Thorlabs optical table equipped with: EM- CCD (Andor, iXonEM$^+$ 897), Argon ion laser (Modu-Laser, Stellar Pro L 300), dichroic (Edmund #86-331), emission filter (Semrock, BLP01-458R-25), 60X objective lens (Nikon, CFI Apo TIRF Oil 60X NA=1.49) and tube lens (Nikon, ITL200 # Thorlabs) [46]. Typical excitation intensity at the sample plane was 50 mW/cm^2 at 458 nm.

2.7. Atomic Force Microscope (AFM) measurements. Samples were prepared by spin casting (3000 rpm, 60 s, acceleration ~ 57 rad/s^2) nanoparticle suspensions (10.7 mg of F8BT/L) on freshly cleaved mica substrates (Grade V-1 Muscovite, SPI). AFM images were obtained on an Agilent 5400 AFM microscope in tapping mode operating at a scan rate of 12.05 microns/s, with resolution of 512x512 pixels and a physical image size of 15x15 microns, using a cantilever (μMasch NSC15/AIBS) with nominal frequency of vibration of 325 kHz, radius of curvature < 10 nm and force constant of 46 N/m. Images (approximately 10 frames per sample) were processed with the Gwyddion program [47]: field curvature effects were first removed using the "Remove Polynomial Background", "Correct lines by matching height median" and "Level data by mean plane subtraction" functions. The resulting images were then analyzed with the same program to select particles using the "Mark grains by threshold" function and finally to obtain the maximum height of each identified particle the "Grain Distributions" function was used. The resulting data was used to build nanoparticle height histograms.

2.8. Dynamic Light Scattering (DLS) measurements. Measurements were performed with a Zeta-Sizer Nano ZS90 Instrument, at a temperature of 25 °C. Light scattering results were analyzed with Zetasizer software (provided by the manufacturer) to obtain hydrodynamic radius distributions by number. Particle suspensions for DLS were prepared with water filtered through 0.2 μm pore filters right before data acquisition. Extreme care was taken to reduce the contamination by dust.

2.9. Estimation of NP molar concentration ([NP]). [NP] was estimated from the F8BT polymer mass concentration (P_{mass}), Avogadro's number (N_A), polymer density (ρ = 0.75 kg/L) [48] and assuming spherical NP with constant diameter (d), according to Eq. 1:

$$[\mathrm{NP}] = \frac{6\,P_{mass}}{d^3 \rho \pi N_A} \qquad (1)$$

With d = 22 nm (average height measured by AFM, see Section 2.7) and P_{mass} = 2.14 mg F8BT/L, we obtain [NP] ~ 0.87 nM.

2.10. Photooxidation of anthracene derivatives. Photooxidation experiments were conducted by placing solutions of ADPA in water or DMA in MeCN, containing CP NP inside a fluorescence cuvette. It is well known that anthracene derivatives with substituents in the 9 and 10 positions, such as ADPA and DMA, react efficiently with $O_2(^1\Delta_g)$ (e.g. the rate for the quenching of $O_2(^1\Delta_g)$ by ADPA water and DMA in MeCN are k_t^{ADPA} = 8.2 x 10^7 M^{-1} s^{-1} and k_t^{DMA} = 8.8 x 10^7 M^{-1} s^{-1}, respectively) to form the corresponding endoperoxides (ADPA-O_2 and DMA-O_2) [33,35,36]. Samples were irradiated either with a wavelength-selective photoexcitation system (PTI, composed of a 75W xenon lamp and a reflection grating monochromator) or with two blue LEDs (λ_{ex}~ 467 nm, FWHM ~ 28 nm, total optical power ~ 14 mW) while simultaneously monitoring the changes in absorbance of ADPA (or DMA) as function of time. It is important to note that the excitation source selectively excites the polymer NP and do not photoexcite either ADPA or DMA. Absorption spectra of the solutions were automatically collected at specific time intervals using a UV-Vis spectrophotometer equipped with a kinetic software module. The molar extinction coefficients of the endoperoxides, ADPA-O_2 in water at 400 nm or DMA-O_2 in MeCN at 377 nm, are considered to be negligible (e.g. $\varepsilon_{DMA\text{-}O2}^{377} < 10$ M^{-1} cm^{-1}) as compared to that of ADPA or DMA in the same conditions (e.g. ε_{DMA}^{377} ~ 10000 M^{-1} cm^{-1}) [37]. Thus, the oxidation reaction (ADPA+ $O_2(^1\Delta_g) \rightarrow$ ADPA-O_2 or DMA+ $O_2(^1\Delta_g) \rightarrow$ DMA-O_2) is conveniently followed by monitoring changes in absorption at 400 nm or 377 nm and directly assigning these changes to variations in ADPA or DMA concentrations, respectively. Kinetic traces were constructed by monitoring the absorption, at the previously mentioned wavelengths, as a function of time (t). Each absorption value was first corrected by subtracting the initial absorption of the sensitizing NP at the same wavelength, and the resulting values were later normalized to the absorption at t = 0 s (Abs_0) and plotted as Abs/Abs_0 *vs.* *t*. Control experiments in the absence of substrate showed that the absorption of NP sensitizers at the measured wavelengths remains constant through the irradiation time. During measurements, ADPA or DMA solutions were continuously purged with either argon or open to the atmosphere as indicated. Argon was previously saturated with water (for ADPA experiments) or MeCN (for DMA experiments) to prevent evaporation of solvent in the reaction cuvette.

2.11. Oxygen consumption. Measurements were carried out with a Clark-type oxygen sensing microelectrode (Lazar, DO-166MT-1). The photosensitized oxidation kinetics of FFA (a $O_2(^1\Delta_g)$ chemical trap) was monitored by measuring consumption of oxygen dissolved in solution during selective photoirradiation of NP. It is well known that FFA reacts specifically with $O_2(^1\Delta_g)$ to yield the corresponding endoperoxide (FFA-O_2) [38]. The dissolved $O_2(^3\sum_{g-})$ concentration in solution was followed potentiometrically with the Clark-type microelectrode as a function of the photoirradiation time. Initial concentrations of NP and FFA were 10.7 mg/L (4.3 nM) and 50 μM, respectively. Microelectrode calibration was performed before each experiment using air saturated water at room temperature.

3. Results

3.1. Particle size distribution. Nanoparticles were prepared as described in the Experimental section and the size distribution was characterized using DLS and AFM. Fig. 1a shows an AFM image of F8BT NP deposited on a mica substrate. In Fig. 1d, the height distribution of particles it is displayed together with a Gaussian fit to the data yielding a mean particle height of 22 nm and σ = 3 nm. Figure 1c shows the hydrodynamic diameter (d_h) distribution ofF8BT NP measured by DLS yielding a mean d_h of ~ 40 nm. The lack of agreement between AFM and DLS results can be rationalized considering that particle height measured over mica surfaces might not be equivalent to its diameter due to potential deformations induced by particle-mica interactions. Additionally, hydrodynamic diameters are usually larger than particle heights measured in dry conditions due to particle solvation shell and particle shape deviations from perfect spherical symmetry assumed in the former [49]. Figure 1b shows a fluorescence micrograph of F8BT NP deposited over a glass coverslip. Diffraction limited fluorescence spots are assigned to the emission from individual NP. Overall the results confirm that the synthesized particles have nanometric dimensions and a relatively narrow size distribution and that are detectable at the single particle level using fluorescence microscopy.

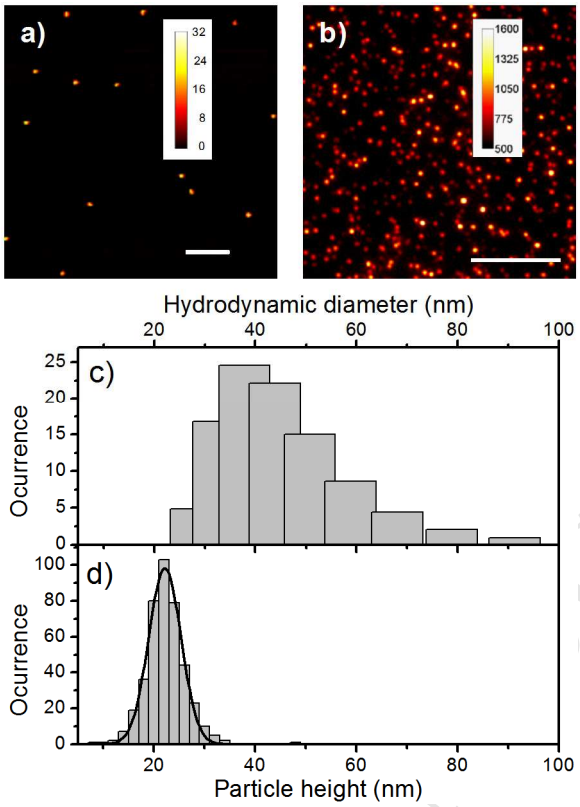

Figure 1. NP characterization: a) AFM micrograph of F8BT NP deposited over a freshly cleaved mica substrate. Scale bar: 1 μm. False color height scale in nm. b) Fluorescence micrograph of F8BT NP deposited over a glass coverslip. Scale bar: 10 μm. False color fluorescence intensity scale in arbitrary counts. c) Hydrodynamic radius size distribution measured by DLS for F8BT NP suspended in water. d) Height distribution (bars) of F8BT NP over mica measured by AFM. The solid line represents the Gaussian fit to the data. See text for details.

3.2. Photophysical and electrochemical characterization. F8BT NP and F8BT-10PtOEP NP were characterized by steady state absorption and steady state and time resolved emission spectroscopy. Fig. 2 shows the absorption and emission spectra of F8BT NP and F8BT-10PtOEP NP suspended in water and those of PtOEP and F8BT in THF solutions. The absorption spectrum of F8BT NP (Fig. 1a, solid black line) is slightly red-shifted compared to that of F8BT in THF solution (Fig. 1b, solid black line). The emission spectrum of the NP (Fig. 1a, dashed black line) is also bathochromically shifted compared to that of the polymer chains in THF (Fig. 1b, dashed black line). The fluorescence quantum yield of F8BT NP suspended in water and that of F8BT dissolved in THF were measured as: $\Phi_F^{NP(H20)} = 0.31$ and $\Phi_F^{THF} = 0.70$,

respectively, in good agreement with previously reported values [50]. The fluorescence decay of F8BT NP in air equilibrated and Ar saturated aqueous suspensions are nearly identical (see Fig. S1) indicating that the singlet excited state of the polymer is not significantly quenched by oxygen. The decay signals were successfully fitted to a biexponential function with τ_1 = 2 ns (60%) and τ_2 = 0.8 ns (40%). From these values, an average lifetime of ~1.52 ns is calculated. In THF the emission of F8BT decays monoexponentially with an associated τ ~ 2.7 ns (data not shown).

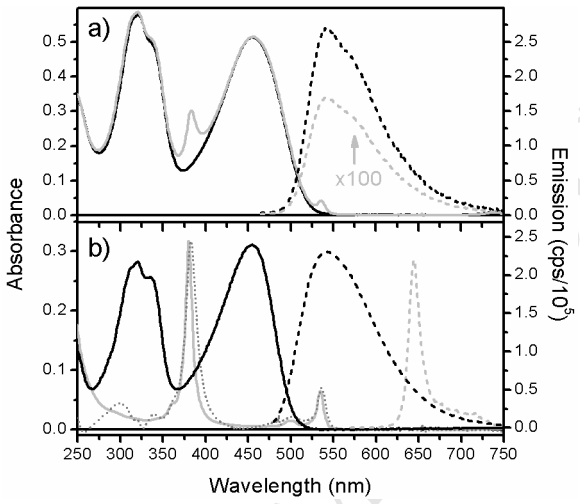

Figure 2. a) Absorption (solid lines) and emission (dash lines) spectra of F8BT NP (black) and F8BT-10PtOEP NP (grey) suspensions in water (Ar saturated). b) Absorption (solid lines) and emission (dash lines) spectra of F8BT (black) and PtOEP (grey) in Ar saturated THF solution. Absorption spectrum of PtOEP in F8BT matrix (grey dotted line) estimated as described in the text.

The absorption spectrum of F8BT-10PtOEP NP (Fig. 2a, solid grey line) clearly shows absorption peaks corresponding to the Soret and Q bands of the porphyrin. The absorption of PtOEP in the F8BT polymer matrix (Fig. 2b, dotted grey line) was estimated by subtracting the absorption spectrum of F8BT NP (Fig. 2a, solid black line) to that of F8BT-10PtOEP NP (Fig. 2a, solid grey line). The resulting spectrum is similar to that of PtOEP in THF solution (Fig. 2b, solid grey line) suggesting good interaction between the polymer matrix and the PtOEP ring, and no evidence for the formation of porphyrin aggregates within the NP. PtOEP aggregation has been previously observed in polystyrene (and other polymer matrixes) at 10% w/w doping and it was evidenced by the appearance of a new absorption peak at ~ 412 nm [51]. The emission spectrum of

the doped NP (Fig. 2a, dashed grey line) is identical in shape to that of F8BT NP, but ~ 100 fold less intense. As expected, the quenching of F8BT emission in the F8BT-#PtOEP NP increases (linearly) with increasing degree of porphyrin doping (Fig. S2). The apparent Stern-Volmer type constant obtained is K_{SVa}= (1800 ± 200) (moles of P8FT monomer units / moles of porphyrin), and it can be interpreted as the number of polymer monomer units quenched by half by the presence of a single PtOEP molecule. This extraordinarily high quenching efficiency has been previously interpreted in analogous systems as consequence of efficient energy transfer among polymer chromophores (exciton diffusion) towards dopant molecules [17,50,52,53]. On the other hand, the excitation of PtOEP in air equilibrated THF solutions generates the porphyrin triplet excited state (^{3}PtOEP) with nearly unitary efficiency [54]. ^{3}PtOEP subsequently decays regenerating the porphyrin ground state by phosphorescence emission (Φ_P = 0.38, τ_P ~ 50-90 µs in deoxygenated THF) [51,54]. The phosphorescence spectrum of ^{3}PtOEP in deoxygenated THF solution is shown in Fig. 2b (dashed grey line). However, for F8BT-10PtOEP NP suspended in deoxygenated water, porphyrin phosphorescence (~ 640 nm) is not observed (see Fig. 2a, dashed grey line).

The energies of first singlet excited states (E_S) of F8BT (^{1}F8BT*) and PtOEP (^{1}PtOEP*) were calculated by averaging the energy of the longest wavelength absorption and shortest wavelength emission maxima. The calculations indicate that ^{1}F8BT* and ^{1}PtOEP* lie at ~2.48 eV and ~2.30 eV above the corresponding ground states, respectively. The energy of the lowest triplet states ^{3}F8BT* (1.62 eV) [55] and ^{3}PtOEP* (2.00 eV) [56] where obtained from bibliography. The reported ^{3}PtOEP energy is consistent with that estimated from the high-energy edge of PtOEP phosphorescence spectrum (grey dashed line in Fig. 2b). The oxidation potential of F8BT in MeCN (+1.65 V *vs.* SCE) was measured by cyclic voltammetry (see Fig. S3). The reduction potential of PtOEP in dichloromethane was reported to be -1.35 V *vs.* SCE [57].

The generation and dynamics of F8BT and PtOEP triplet excited states upon excitation of undoped and doped NP was investigated using the laser flash photolysis technique. Fig. 3 shows the transient (difference) absorption spectra of F8BT in THF (circles) and F8BT NP suspended in water (squares). Samples were deoxygenated as described in the experimental section. The transient spectrum of F8BT in THF shows positive transient absorption between 500-850 nm and a negative transient absorption band centered ~ 450 nm. The transient negative absorption signal matches well the absorption spectrum

of F8BT in THF (black solid line, Fig. 3) and therefore, it is assigned to the bleaching of the polymer ground state. The inset in Fig. 3 shows that the kinetic absorption profiles obtained at 460 nm (ground state recovery) and 740 nm follow a first order kinetics with identical lifetimes (~ 120 μs). This agreement indicates that repopulation of the ground state occurs by decay of the species responsible for the transient absorption between 500-850 nm. Furthermore, since both transient absorptions disappear when the experiment is carried-out in the presence of oxygen, the positive transient absorption signal at λ > 500 nm is assigned to the triplet excited state of the polymer ($T_1 \rightarrow T_n$ transitions) and thus, the 120 μs decay component is associated with ^{3}F8BT* lifetime (τ_T).

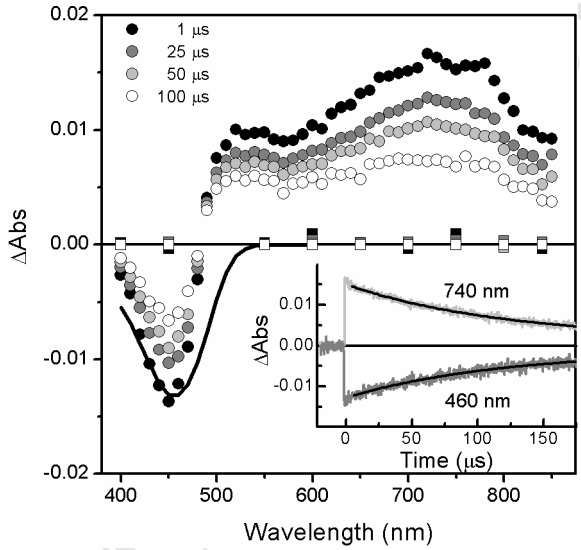

Figure 3. Time evolution of the transient absorption spectra of deoxygenated solutions of F8BT in THF (circles) and F8BT NP in water (squares) observed at: 1 (black), 25 (dark grey), 50 (light grey) and 100 (white) μs after the laser pulse (355 nm, FWHM~ 15 ns, PP ~ 2 mJ). The black solid line shows the normalized inverted steady state absorption of F8BT in THF. Inset: kinetic profiles observed at 460 nm (dark grey line, F8BT ground state recovery) and 740 nm (light grey line, F8BT triplet excited state decay) and exponential fit to the data (black lines)

Using the ground state depletion (GSD) method [59] the absorption coefficient of ^{3}F8BT* was estimated as $\varepsilon_T^{740} \sim 54$ L g^{-1} cm^{-1}. Unexpectedly, no transient absorption is observed for F8BT NP in deoxygenated water (see Fig. 3, squares) when studied in the same time window **(**~1-200 μs). Analogous results were obtained for F8BT-10PtOEP

NP where no evidence was found either for the formation of ^{3}F8BT* or the porphyrin triplet excited state. ^{3}PtOEP* has been reported to show a strong transient triplet-triplet absorption around 400-490 nm and a less intense band at 550-700 nm [60]. A mechanism that accounts for the lack of triplet excited states formation in the NP suspensions is discussed in Section 5.

The most relevant photophysical properties of F8BT and PtOEP in TFH solutions and of doped and undoped F8BT NP suspensions in water (or D_2O) are collected in Table 1.

Table 1. Photophysical, photochemical and electrochemical properties of F8BT doped and undoped NP

	F8BT (in THF)	**PtOEP (in THF)**	**F8BT NP (in water)**	**F8BT-10PtOEP NP (in water)**
E_S (eV)	2.48	2.30	(2.48)	(2.30)
E_T (eV)	1.62	2.00	(1.62)	(1.62)
Φ_F	0.75	-	0.32	<0.01
Φ_P	n.o.	0.38[e]	n.o.	n.o.
τ_S (ns)	2.7	-	1.52	n.o.
τ_T (μs)	120	50-99[e]	n.o.	n.o.
E_{oxi} (V *vs.*SCE)	+1.65[c]	-	(+1.65)	-
E_{red} (V *vs.* SCE)	-1.99[c]	-1.35[f]	-	(-1.35)
Φ_Δ[a]	0.07[d]	~1.00[g]	0.09[h]	0.24[h]
Φ_Δ[b]	-	-	0.22[h]	0.66[h]

n.o.: not observed.
[a] Quantum yield for $O_2(^1\Delta_g)$ sensitization obtained from steady state emission spectroscopy.
[b] Quantum yield for $O_2(^1\Delta_g)$ sensitization obtained from ADPA consumption experiments.
[c] films over Pt electrode in MeCN, see Supporting Information for details.
[d] in aerated benzene from reference [58].
[e] from references [51,54].
[f] in dichoromethane from reference [57].
[g] estimated from reference [54] assuming that ^{3}PtOEP* quenching by $O_2(^3\Sigma_g^-)$ is dominated by energy transfer leading to the formation of $O_2(^1\Delta_g)$.
[h] in aerated D_2O.

3.3. Photosensitized $O_2(^1\Delta_g)$ generation by F8BT and F8BT-PtOEP NP.

3.3.1. $O_2(^1\Delta_g)$ phosphorescence measurements. Direct evidence of the formation of $O_2(^1\Delta_g)$ upon irradiation of nanoparticles in D_2O were obtained by steady state emission spectroscopy. These measurements allow to determine directly the presence of $O_2(^1\Delta_g)$ by detecting its characteristic phosphorescence in the near infrared (NIR) spectral range (maximum at ~ 1268 nm [61]). Fig. 4 shows the $O_2(^1\Delta_g)$ stationary emission spectrum of a F8BT NP and F8BT-10PtOEP NP suspensions in D_2O upon excitation at 487 nm. NP fluorescence background signals were obtained from similar experiments in Ar

saturated solutions. Relative quantum yields for $O_2(^1\Delta_g)$ generation (Φ_Δ) were estimated by comparing the phosphorescence intensities measured for NP samples with those produced by Eosin Y (Φ_Δ = 0.58 in D_2O) [44]. From these experiments, values of Φ_Δ ~ 0.09 and 0.24 were obtained for F8BT NP and F8BT-10PtOEP NP, respectively. A value of Φ_Δ ~0.07 has been previously reported for F8BT in benzene [58].

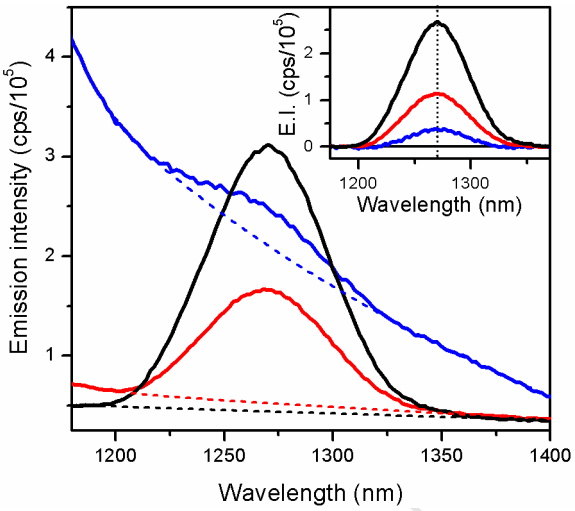

Figure 4. Steady-state emission spectrum in the NIR region generated by Eosin Y (black solid line), F8BT NP (green solid line) and F8BT-10PtOEP NP (red solid line) in aerated D_2O solutions. NP fluorescence emission backgrounds are shown as dashed lines, see SI for details. Inset: $O_2(^1\Delta_g)$ emission spectrum obtained by subtraction of the sample signals and the corresponding fluorescence backgrounds. The vertical dotted line shows the emission maximum at ~ 1268 nm.

3.3.2. Substrate consumption. Approximated values of Φ_Δ can be also estimated by studying the rate of oxidation of organic substrates (ADPA or DMA) by $O_2(^1\Delta_g)$ [33,35–37]. In this case, F8BT NP or F8BT-10PtOEP NP act as the $O_2(^1\Delta_g)$ photosensitizers (S). Figure 5a shows the consumption of ADPA in the presence of F8BT NP (blue dots), F8BT-10PtOEP NP (red dots) and the reference Eosin Y (EY) (black dots) as a function of irradiation time with (quasi)monochromatic light at 487 nm. These changes are associated with the photosensitized production of $O_2(^1\Delta_g)$ by the NP and subsequent oxidation of ADPA to give the corresponding endoperoxide (ADPA-O_2, Fig. 5a inset). Formation of DMA-O_2 as the main photoproduct (> 95%,) upon irradiation of F8BT NP in acetonitrile was confirmed by HPLC (see Fig. S4). Accordingly, ADPA is not consumed when experiments are carried-out on suspensions saturated with Ar. Control experiments in the absence of sensitizer (not shown)

demonstrate that auto-photosensitization of ADPA is negligible under the experimental conditions due to the lack of significant absorption of ADPA at the excitation wavelength (487 nm). As shown in Fig. 5a, ADPA consumption in samples with F8BT-10PtOEP NP is faster than in samples of undoped F8BT NP. Furthermore, the velocity of ADPA consumption clearly increases with increasing degree of porphyrin doping of the F8BT particles as shown in Fig. S5. Figure 5c shows the absorption spectra of ADPA in the presence of F8BT-10PtOEP NP before (black line) and after irradiation for 1500 s (grey line). In both cases, the spectrum of the NP remains unchanged after irradiation (compare black and grey lines above 420 nm) suggesting that these particle sensitizers are resistant to ROS induced oxidation/degradation processes usually seen for conventional photosensitizers.

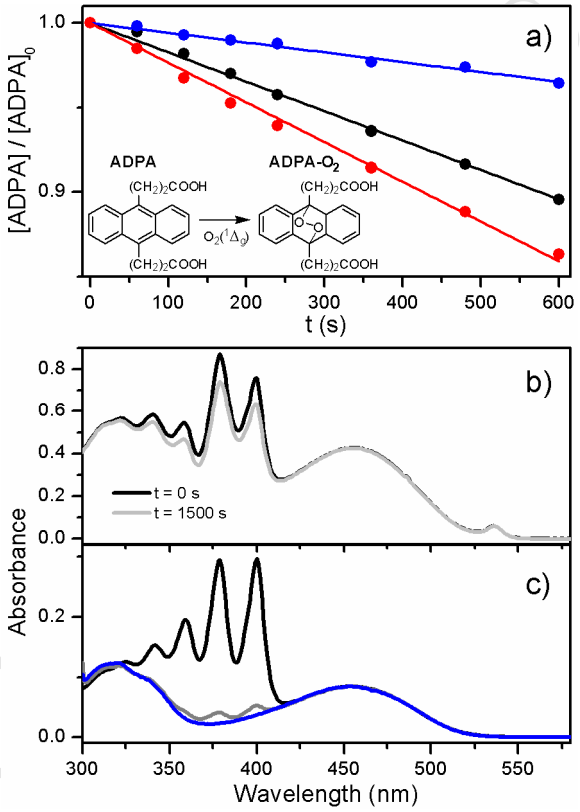

Figure 5. a) ADPA consumption as a function of irradiation time (λ_{ex} = 487nm, using a wavelength-selective photoexcitation system, see experimental section for details) in presence of F8BT NP (red circles) and F8BT-10PtOEP NP (blue circles) and Eosin Y (black circles) in air equilibrated water suspensions and corresponding linear fits. $[ADPA]_0$ = 40 µM, [NP] ~ 4.3 nM and [EY] ~ 10 µM. Inset: Reaction of ADPA with $O_2(^1\Delta_g)$ to yield ADPA-O_2, b) Absorption spectra of sample containing ADPA and F8BT-10PtOEP NP at 0 s (black line) and after 1500 s (grey line) of irradiation. c)

Absorption (black line) and emission-excitation (gray line) spectra of F8BT NP suspended in water (~2 mg/L) with ADPA (~20 μM) and emission-excitation spectrum of F8BT NP suspended in neat water (solid black line). Excitation spectra were collected by monitoring emission at 590 nm and were normalized to the absorption peak of F8BT NP (456nm).

Scheme 2 shows a simplified mechanism for the oxidation of ADPA (*A*) photosensitized by NP (S). Assuming steady state for $[O_2(^1\Delta_g)]$, the initial rate (v_0) for ADPA consumption is given by Eq. 2 *[62]*:

$$v_0 = -\left(\frac{d[A]}{dt}\right)_0 = \frac{k_r \tau_0 [A]_0 \Phi_\Delta I_a}{1 + k_t \tau_0 [A]_0} \qquad (2)$$

where $[A]_0$ is the initial substrate concentration, Φ_Δ is the quantum yield of $O_2(^1\Delta_g)$ generation, I_a is the intensity of light absorbed at the excitation wavelength, τ_0 ($1/k_d$) is the lifetime of $O_2(^1\Delta_g)$ in the absence of substrate, k_r is the reaction rate constant of $O_2(^1\Delta_g)$ associated exclusively with formation of endoperoxide (A-O_2) and k_t is the total rate constant of $O_2(^1\Delta_g)$ quenching ($k_t = k_r + k_q$, where k_q is the physical deactivation rate constant of $O_2(^1\Delta_g)$ induced by the substrate).

$$\begin{aligned}
S &\xrightarrow{I_a} {}^1S^* \\
{}^1S^* &\xrightarrow{k_{isc}} {}^3S^* \\
{}^3S^* + O_2(^3\Sigma_g^-) &\xrightarrow{k_{TET}} {}^1S^* + O_2(^1\Delta_g) \\
A + O_2(^1\Delta_g) &\xrightarrow{k_r} A\text{-}O_2 \\
A + O_2(^1\Delta_g) &\xrightarrow{k_q} A + O_2(^3\Sigma_g^-) \\
O_2(^1\Delta_g) &\xrightarrow{k_d} O_2(^3\Sigma_g^-)
\end{aligned}$$

Scheme 2. Simplified mechanism for photosensitized ADPA oxidation.

Experiments were designed so that the rate of photon absorption (I_a) by all samples is identical (and constant) during irradiation (see Fig. S6), additional details are provided in the SI. Considering that in water $k_t\tau_0 \sim 2.5\text{x}10^2$ M^{-1} [62] and $[A]_0 = [\text{ADPA}]_0 = 50$ μM, it follows that $k_t\tau_0[A]_0 << 1$. Thus, for the experiments shown in Fig. 5a, v_0 can be written as:

$$v_0 = -\left(\frac{d[A]}{dt}\right)_0 \cong k_r \tau_0 [A]_0 \phi_\Delta I_a \qquad (3)$$

which allows to calculate relative Φ_Δ according to: $v_0^{NP}/v_0^{EY} \sim \Phi_\Delta^{NP}/\Phi_\Delta^{EY}$. Hence, taking into account that in air equilibrated water solutions $\Phi_\Delta^{EY} = 0.57$ *[63]*, values of $\Phi_\Delta \sim 0.22$ and ~0.66 are calculated for F8BT NP and F8BT-10PtOEP NP, respectively. Surprisingly, these Φ_Δ are ~3 times larger than those estimated directly from $O_2(^1\Delta_g)$ phosphoresce (Section 3.3.1). Thus, we conclude that either the mechanism assumed for NP photoinduced oxidation of ADPA (Scheme 2) or the approximations leading to Eq. 3 must be incorrect. Similar conclusions were reached by studying the solvent isotopic effects on the oxidation process, see Fig. S7. Isotopic effects are primarily associated with the differences in intrinsic lifetimes of $O_2(^1\Delta_g)$ in the studied solvent. According to Eq. 3, the ratio of the initial oxidation rates measured in D_2O and H_2O should be: $v_0^{D2O}/v_0^{H2O} \cong \tau_0^{D2O}/\tau_0^{H2O} \sim 10$ *[64,65]*. However, the experimental $v_0^{D2O}/v_0^{H2O} \sim 2$ (see Fig. S8) is significantly smaller than the expected. To further investigate this unusual behavior of F8BT NP as photosensitizers, the dependence of v_0 on the initial concentration of ADPA was studied in H_2O and MeCN. Note that Eq. 2 can be rewritten as:

$$v_0^{-1} = (k_r \tau_0 \phi_\Delta I_a)^{-1}\left(1 + \frac{k_t \tau_0}{[A]_0}\right) \qquad (4)$$

thus, a plot of v_0^{-1} *vs.* $[A]_0^{-1}$ can be used to estimate the value of $k_t\tau_0$. Such plots are shown in Fig. S8. Fitting the experimental data to Eq. 4, provides values of $k_t\tau_0 \sim 1.3\text{x}10^4$ M^{-1} and $\sim 5.2\text{x}10^4$ M^{-1} for the oxidation of ADPA by $O_2(^1\Delta_g)$ in H_2O and MeCN, respectively. Interestingly, although the double reciprocal plots are linear, the calculated $k_t\tau_0$ are considerably larger than those reported previously for the oxidation of ADPA by $O_2(^1\Delta_g)$; *i.e.* $k_t\tau_0 \sim 2.5\text{x}10^2$ M^{-1} (in H_2O) and $7.1\text{x}10^3$ M^{-1} (in MeCN) [62]. At this point, we speculate that the adsorption of ADPA on the NP surface could explain these unexpected results, this hypothesis will be tested and discussed in detail in Section 3.4.1.

3.3.3. Molecular oxygen consumption. This method evaluates the kinetics of photosensitized oxidation of FFA by measuring consumption of molecular oxygen in the ground state ($O_2(^3\Sigma_g^-)$) dissolved in solution during selective photoirradiation of F8BT-NP or F8BT-10PtOEP NP. Furfuryl alcohol reacts with $O_2(^1\Delta_g)$ as shown in Fig.

7 (insert) consuming $O_2(^3\Sigma_g^-)$ and generating FFA-O_2 which is thermally unstable and acts as an intermediate for the formation of oxidation products [38,39]. $O_2(^3\Sigma_g^-)$ concentration was measured potentiometrically, using a specific microelectrode, as a function of irradiation time. The results are shown in Fig. 7. For both samples containing FFA and F8BT NP or F8BT-10PtOEP NP a considerable oxygen consumption (dash traces) is observed in a brief period which can be attributed to the photosensitized generation of $O_2(^1\Delta_g)$ by the NP and subsequent reaction with FFA. Samples containing F8BT-10PtOEP NP show faster $O_2(^3\Sigma_g^-)$ consumption than those with F8BT NP consistently with substrate consumption experiments. Additional oxygen consumption experiments were run in NP suspension without FFA to evaluate the photochemical stability of the particles against $O_2(^1\Delta_g)$. The results of these experiments (Fig. 7, solid lines) show that under these conditions oxygen concentration does not change suggesting that $O_2(^1\Delta_g)$ generated during photoirradiation of NP does not chemically react with the NP to give oxidized products. These observations are consistent with the lack of significant particle absorbance bleaching in substrate consumption experiments (Section 3.5) confirming the excellent photostability of the developed NP sensitizers.

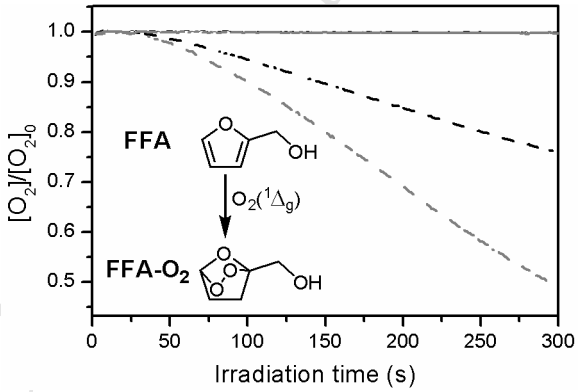

Figure 7. Molecular oxygen consumption as a function of irradiation time for water suspensions of F8BT NP (black lines) or F8BT-10PtOEP NP (grey lines) in the presence (dashed lines) and absence (solid lines) of FFA. [NP] = 6 mg/L, [FFA] = 50 μM. Insert: Reaction of FFA with $O_2(^1\Delta_g)$ to yield FFA-O_2. Selective NP irradiation was provided by blue LEDs, see experimental section for details.

3.4. Adsorption of water soluble organic molecules onto F8BT NP.

3.4.1. ADPA adsorption. As mentioned in Section 3.3.2, the unexpected results obtained for the oxidation of ADPA photosensitized by F8BT NP suggested adsorption of the substrate onto the particles. If a fraction of ADPA is bound to the NP, the resulting increased local [ADPA] at the NP surface (where $O_2(^1\Delta_g)$ is generated) should favor $O_2(^1\Delta_g)$ trapping. This is equivalent to considering that the apparent concentration of ADPA found by $O_2(^1\Delta_g)$ is larger than $[A]_0$, making the approximation $k_t \tau_0 [A]_0 << 1$ invalid (see Section 3.3.2, Eq. 2 and Eq. 3). To test this hypothesis, we studied the energy transfer (ET) from ^{1}ADPA* to F8BT NP using steady state absorption and fluorescence spectroscopy. Figure 5c shows the absorption (black line) and corrected emission excitation spectra (grey line, collected at 550 nm where only F8BT emits) of an aqueous solution containing F8BT NP (~2 mg/L) and ADPA (~20 μM). The excitation spectrum of F8BT NP suspended in water without ADPA is also shown for comparison (blue line). The corrected excitation spectrum in presence of ADPA (solid grey line) clearly shows spectral features of ADPA absorption (peaks in the 350-410 nm region) confirming the occurrence of the singlet-singlet ET process. This ET process can occur through Förster or Dexter mechanisms, for the latter being necessary that APDA and F8BT NP to be essentially in contact (to achieve optimal wavefunction overlap between reactants) *[66]*. On the other hand, for Förster ET to be effective, ADPA and F8BT NP must be (on average) at a distance close or below the Förster radius (R_0). Based on previous considerations, a critical energy acceptor concentration ($[C]_c$) can be defined below which Förster ET between freely diffusing molecules in solution is negligible. Equation 5 describes the relationship between $[C]_c$ and R_0 *[67]*.

$$[C]_c = \frac{3000}{2\pi^{3/2} N_A R_0^3} \qquad (5)$$

where N_A is Avogadro's number and $[C]_c$ is given in mol/L when R_0 is expressed in cm. Using this equation and assuming an upper limit of 100 Å for R_0 in our system (typical R_0 values for donor/acceptor pairs where ET is highly efficient are < 100 Å) [68] we calculate $[C]_c$ > 0.45 mM. Since the estimated F8BT NP concentration ([NP] < 0.87 nM, Section 2.9) is more than six orders of magnitude lower than $[C]_c$ we conclude that ADPA and F8BT NP in these experiments are not independently diffusing in solution but that (at least) a fraction of the ADPA must be adsorbed to the NP to account for the observed ET process. The nature of the ADPA/NP adsorption process is not easy to explain, particularly considering that at neutral pH, F8BT NP are negatively charged

(the zeta-potential has been determined to be –(26±2) mV in deionized water [69]) and that a significant fraction of ADPA (α~0.5) must be ionized. To study the ET from ^{1}ADPA* to F8BT NP process and the adsorption phenomenon in more detail, additional experiments were performed measuring fluorescence excitation spectra at various ADPA analytical concentrations ($[A^i]_0$) (see SI for details and Fig. S9). The results were interpreted assuming the Langmuir model, according to Eq 6 [70]:

$$\frac{[A]_{free}}{A_{ad}} = \frac{1}{NK_{ad}} + \frac{[A]_{free}}{N} \qquad (6)$$

where A_{ad} are the moles of ADPA adsorbed onto the surface of the NP per gram of F8BT and $[A]_{free}$ is the molar concentration of free (non-bound) ADPA, K_{ad} is the (average) associated adsorption equilibrium constant and N is the (average) moles of binding sites per gram of F8BT. A_{ad} and $[A]_{free}$ can be calculated (see details in the SI) from fluorescence excitation experiments (assuming 100% energy transfer efficiency from excited A_{ad} to F8BT), $[A]_0$ and the solution volume (V). From this data a modified Langmuir plot ($[A]_{free}/A_{ad}$ *vs.* $[A]_{free}$) was constructed (Fig. 6) and a linear fit to the data using Eq. 6 was used to calculate N = (5.5±0.7) x 10^{-3} $mol_{(sites)}/g_{(F8BT)}$ and K_{ad} = (8±1) x 10^3 M^{-1}. Considering that in these experiments the estimated concentration of NP is 0.87 nM, the (average) number of adsorption sites per NP must be ~14000. Figure 6 inset shows a plot of the (molar) concentration of ADPA "sequestered" by the NP ($[A]_{ad}$ = $[A]_0$ -$[A]_{free}$), as a function of the analytical concentration of $[A]_0$. As shown, the plot is linear within the interval of $[A]_0$ studied (from 6 to 40 μM). This result is important since it explains the linear dependence of v_0^{-1} *vs.* $[A]_0^{-1}$ plots shown in Fig. S7. This is, the apparent concentration of ADPA bound to the NP surface is a (nearly) constant fraction of $[A]_0$. In the inset of Fig. 6, it is also shown that the dependence of the occupied binding sites' fraction ($\theta = A_{ad}/N$) with $[A]_0$. The plot is linear suggesting that the equilibrium is in the linear regime of the Langmuir isotherm.

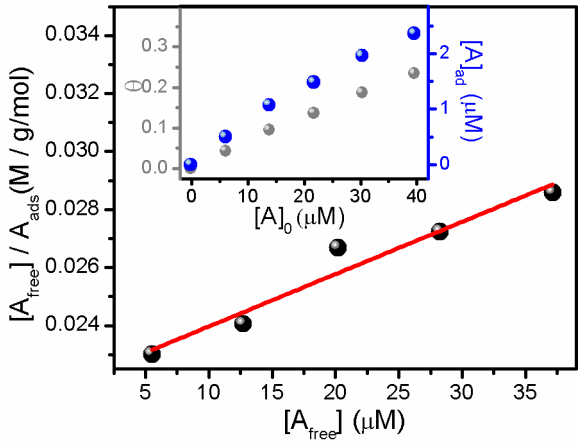

Figure 6. Modified Langmuir plot for the adsorption of ADPA on the surface of F8BT NP. Insert: dependence of the fraction of F8BT occupied sites (θ, grey data points) and the molar concentration of sequestered ADPA (see text for details) with $[A]_0$.

3.4.2. Dye adsorption. Further evidence of the unusual capacity of F8BT NP to adsorb water-soluble organic molecules was obtained by studying the quenching of F8BT NP fluorescence by zwitterionic, anionic and cationic dyes. The structure of the dyes used for these studies are shown in Scheme 1. Details for these experiments are discussed in detail in the SI. As shown in Fig. S10, addition of RhB to a F8BT NP suspension in water leads to the efficient quenching of the NP emission (540 nm) together with the appearance of dye emission at ~577 nm. A simple Stern-Volmer treatment of the experimental data (inset Fig. S10) at concentrations of [RhB] < 15 nM, shows a "superquenching" effect [5] producing an apparent Stern-Volmer constant of $K_{SV\text{-}RhB}$ = 5.8 x10^7 M^{-1}. Comparable results were obtained for the quenching by RB and MB, yielding $K_{SV\text{-}RB}$ = 4.5x10^7 M^{-1} and $K_{SV\text{-}MB}$ = 1.7x10^7 M^{-1}, respectively (see Fig. S11 and Fig. S12) . Considering Eq. 5 and the low concentrations of NP ([NP] = 0.87 nM) and dye-quenchers ([Q] ≤ 0.3 μM) used in these experiments, it can be concluded that the significant quenching observed must be due to the adsorption of the quencher dyes (Q) to the NP surface. Therefore, these experiments corroborate that the NP can adsorb different substrates independently of their net charges. Interestingly this efficient adsorption of a wide range of water soluble (ionic) dyes (present at very low concentrations) onto F8BT NP in aqueous suspension provides a simple and versatile method to achieve superficial dye-doping of these particles. Moreover, this type of doping favours vectorial energy transfer from the particle core towards its (dye decorated) surface. Thus such NP systems display high photon collection capacity and

efficient funnelling of excitation energy towards the particle surface can be useful in applications requiring a high flux of readily available excitation energy to drive physical or chemical transformations.

4. Discussion.

The experiments described in Section 3 demonstrate that the studied NP have a rich and complex photophysics. In conjugated polymers, the effective length of the delocalized orbital associated with a π-π* transition is usually assumed to be restricted to chain segments containing only few monomer repeat units. Each of these segments is considered a chromophore and the associated excited state a molecular (or Frenkel) exciton [71,72]. Thus, each polymer chain is formed by a series of linked independent chromophores having different conjugation lengths. The photophysical properties of individual polymer chains and NP (composed by one or many collapsed chains) are affected by several conformation-dependent factors including: chromophores´ conjugation-length and spatial distribution, and energy and electron transfer among nearby chromophores (also described as exciton diffusion) [73]. As shown in Table 1, the Φ_F and τ_F of undoped F8TB NP suspension in water are smaller than the observed for the conjugated polymer in THF (Table 1). This is attributed to fast intra-particle energy transfer processes that allow efficient funneling of excitation energy to weakly fluorescent polymer "traps" acting as fluorescence quenchers [50]. These energy transfer/quenching processes are favored by the folding and close packing of the polymer chains upon nano-aggregates formation. The complex emission decay observed also agrees with the existence of an assembly of fluorophores affected by different deactivation processes. Similar behavior has been described for many other micro-heterogeneous systems [45]. F8BT NP capacity to generate $O_2(^1\Delta_g)$ is small and similar to that observed for F8BT in benzene (Table 1). The detected $O_2(^1\Delta_g)$ must arise from the quenching of ^{3}F8BT* by molecular oxygen. However, ^{3}F8BT* formation in F8BT NP cannot be detected in the flash photolysis experiments (Fig. 3). The lack of ^{3}F8BT* transient signals can be rationalized considering that, after multiple photon excitation, triplet excitons annihilate efficiently due to the confined nature of the NP system. Excited states annihilation processes in F8BT NP (and other conjugated polymer NP) have been already reported in the literature [74–77]. Triplet-triplet (T-T) annihilation are second order (diffusion controlled) reactions and therefore, the rate of these

processes depend on the laser energy (strictly, on I_a^2). In fluid media, T-T annihilation is observed even at moderate laser intensities. In the confined NP system, fast T-T annihilation must be occurring in a time scale not accessible with our flash-photolysis equipment (< 200 ns) leading to a maximum concentration of approximately one triplet exciton per particle [74–78]. The singlet exciton size (conjugation length) of F8BT has been estimated as ~5 monomeric units [74,79]. If singlet and triplet exciton sizes are approximately the same and considering the maximum triplet concentration equal to the particle concentration (~10^{-9} M) the maximum expected transient absorption signal (after the annihilation process) for ^{3}F8BT* NP is estimated to be $\Delta A \sim 6 \times 10^{-4}$ (see details in SI), which is clearly below the detection limit of our instrument. As mentioned before, T-T annihilation processes should be only important in laser flash photolysis experiments. At the low irradiation intensities used in stationary photolysis experiments with LEDs irradiation, most ^{3}F8BT* should survive and be available for quenching by O_2.

The model proposed for the interpretation of the kinetic and spectroscopic data of F8BT-10PtOEP NP is shown in Scheme 3, which displays the relevant high-energy states (Table 1) and kinetic pathways for the system. When excited with blue light (456 nm), F8BT-PtOEP NP preferentially form the ^{1}F8BT*-PtOEP singlet excited state ($h\nu$, Scheme 3). As shown in Fig. 2a, in the presence of PtOEP, the emission of the polymer is almost completely quenched. Possible deactivation mechanisms for ^{1}F8BT*-PtOEP are electron transfer (eT) and ET processes (Scheme 3). The energy of the F8BT$^{\bullet+}$-PtOEP$^{\bullet-}$ charge-separated state was estimated to be at ~ 2.9 eV (disregarding Coulombic and solvation effects) based on the oxidation and reduction potentials collected in Table 1. This energy lies ~ 0.4 eV above ^{1}F8BT*-PtOEP, thus quenching of the polymer singlet excited state *via* an electron transfer mechanism (k_{CT}, Scheme 3) should not be significant. On the other hand, the good spectral overlap between ^{1}F8BT* emission and PtOEP absorption (see Fig. 2a and 2b) suggests efficient singlet-singlet energy transfer from ^{1}F8BT* to the tetrapyrrole ring, yielding ^{1}PtOET* ($k_{SS\text{-}ET}$, Scheme 3) as the possible quenching mechanism. Intersystem crossing is highly efficient in ^{1}PtOET* ($\Phi_{ISC} \sim 1$) [54] thus F8BT-^{1}PtOET* is assumed to decay almost exclusively through this path yielding F8BT-^{3}PtOET* ($k_{ISC,2}$ Scheme 3). As mentioned before, in (deoxygenated) THF solution ^{3}PtOEP* decays efficiently to regenerate the ground state by emission of phosphorescence (Φ_P = 0.38 [54] k_P, Scheme 3). However, in

deoxygenated F8BT-PtOEP NP water suspensions porphyrin phosphorescent emission is not observed (see Fig. 1a) suggesting that F8BT-^{3}PtOEP* must be efficiently deactivated by another mechanism. Taking into account that the energy of the triplet excited state of F8BT (E_T ~ 1.62 eV, Table 1) is lower than that of PtOEP (~ 2.00 eV), a triplet-triplet energy transfer process to give ^{3}F8BT*-PtOEP NP ($k_{TT\text{-}ET}$, Scheme 3) would be thermodynamically favorable, explaining the lack of detection of the F8BT-^{3}PtOEP* emission signal. As explained before, attempts to confirm the formation of ^{3}F8BT*-PtOEP using transient absorption spectroscopy were unsuccessful, presumably because a fast T-T annihilation process takes place under the photoirradiation conditions used in the flash photolysis experiments. At this point, it seems interesting to compare the mechanism of $O_2(^1\Delta_g)$ generation proposed here for F8BT-PtOET NP with that proposed by Wu *et al.* for F8BT-TPP NP. [25,26]. According to these authors, F8BT TPP NP generate $O_2(^1\Delta_g)$ from ^{3}TPP*. In principle, this mechanism can be justified thermodynamically considering that E_T of TPP (~1.44 eV) *[80–82]* is much lower than that of F8BT (E_T (^{3}F8BT*) ~1.62 eV), so ^{3}TPP* must be the lowest-lying triplet state in TPP-doped F8BT NP.

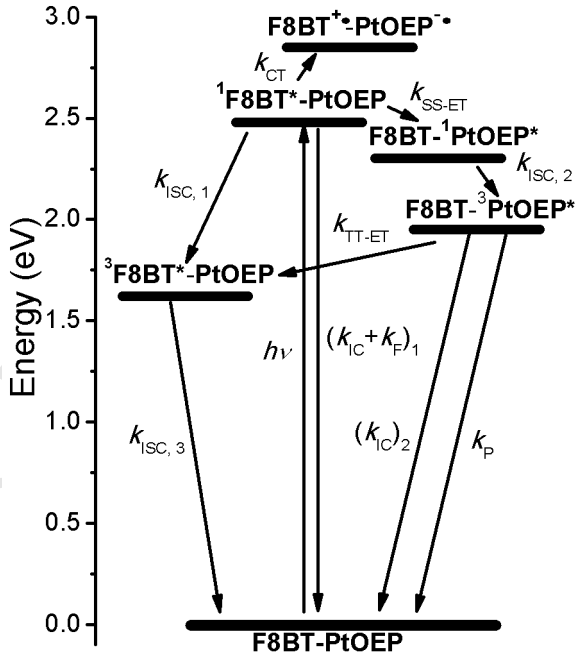

Scheme 3. F8BT-PtOEP NP energy diagram.

The higher Φ_Δ of F8BT-PtOEP NP relative to that of F8BT NP (Table 1) is rationalized considering also the model described in Scheme 3. The presence of porphyrin in these NP increases the formation yield of ^{3}F8BT* via a sequential ET mechanism involving

the following steps: i) S-S ET (^{1}F8BT*-PtOEP$\rightarrow$ F8BT-^{1}PtOEP*), ii) intersystem crossing (F8BT-^{1}PtOEP* $\rightarrow$ F8BT-^{3}PtOEP*) and iii) T-T ET (F8BT-^{3}PtOEP* $\rightarrow$^{3}F8BT*-PtOEP). In turn, the resulting high ^{3}F8BT* quantum yield leads to increased singlet oxygen sensitization efficiency.

It is important to note that although the Φ_Δ (0.24) of F8BT-PtOET NP is not particularly high, the particles display a remarkably high efficiency as sensitizers in the photooxidation of singlet-oxygen chemical-trap substrates (ADPA and DMA). This effect is a consequence of substrate adsorption on the NP surface increasing its local concentration and accelerating its oxidation rate. Furthermore, for analogous particles our group has confirmed a related high efficiency as sensitizers in Photo Dynamic Therapy (PDT) inducing death in cancer cell lines (*in vitro*), these results will be published elsewhere.

5. Conclusions

In summary, we reported on the synthesis and characterization of F8BT NP doped with PtOEP able to efficiently photosensitize the formation of $O_2(^1\Delta_g)$. The mechanism of $O_2(^1\Delta_g)$ generation was investigated in detail by using absorption and emission stationary and time-depend techniques. The quantum yields for $O_2(^1\Delta_g)$ generation sensitized by doped and neat NP were calculated using direct and indirect methods. The results indicate that that for these conjugated polymer NP sensitizers indirect methods, based on evaluation of oxidation rates of $O_2(^1\Delta_g)$ chemical traps, tend to overestimate the Φ_Δ. Conclusive evidence is provided to show that the discrepancy in Φ_Δ obtained from direct and indirect methods is due to the adsorption of the $O_2(^1\Delta_g)$ chemical traps on the NP surface. Furthermore, we present unequivocal evidence for the adsorption of a variety of water soluble dyes onto the NP surface indicating that adsorption of ionic organic molecules on these particles in highly dilute conditions is a common phenomenon that might be exploited for the preparation of superficially dye doped conjugated polymer nanoparticles. These superficially doped particles might be particularly interesting in applications requiring high photon collection and vectorial energy funneling to efficiently generate excitation energy on the particle surface where is readily available.

Acknowledgments

Authors acknowledge financial support of this work by grants from ANPCyT, Argentina (PICT 214/14); CONICET, Argentina (PIP 11220150100295 /2015) and Secretaría de Ciencia y Técnica (SECyT), UNRC (PPI 2016) Argentina. L.P.M., C.L., C.A.C. and R.E.P. are permanent research staff of CONICET. L.I.H. and L.I. thank CONICET for postdoctoral scholarships. R.M.S. and R.A.P thank CONICET for PhD scholarships.

Competing interests

The authors declare no competing financial interest.

References and notes

[1] Günes S, Neugebauer H, Sariciftci NS. Conjugated Polymer-Based Organic Solar Cells. Chem Rev 2007;107:1324–38. doi:10.1021/cr050149z.
[2] Coakley KM, McGehee MD. Conjugated Polymer Photovoltaic Cells. Chem Mater 2004;16:4533–42. doi:10.1021/cm049654n.
[3] Yamada T, Tsubata Y. Recent Progress and Future Perspectives of Light Emitting Polymers for Full-color Display. J Synth Org Chem Jpn 2012;70:473–9. doi:10.5059/yukigoseikyokaishi.70.473.
[4] Chen L, McBranch DW, Wang H-L, Helgeson R, Wudl F, Whitten DG. Highly sensitive biological and chemical sensors based on reversible fluorescence quenching in a conjugated polymer. Proc Natl Acad Sci 1999;96:12287–92. doi:10.1073/pnas.96.22.12287.
[5] Achyuthan KE, Bergstedt TS, Chen L, Jones RM, Kumaraswamy S, Kushon SA, et al. Fluorescence superquenching of conjugated polyelectrolytes: applications for biosensing and drug discovery. J Mater Chem 2005;15:2648–56. doi:10.1039/B501314C.
[6] Rahman MA, Kumar P, Park D-S, Shim Y-B. Electrochemical sensors based on organic conjugated polymers. Sensors 2008;8:118–141.
[7] Wu C, Bull B, Christensen K, McNeill J. Ratiometric Single-Nanoparticle Oxygen Sensors for Biological Imaging. Angew Chem Int Ed 2009;48:2741–5. doi:10.1002/anie.200805894.
[8] Shi H, Ma X, Zhao Q, Liu B, Qu Q, An Z, et al. Ultrasmall Phosphorescent Polymer Dots for Ratiometric Oxygen Sensing and Photodynamic Cancer Therapy. Adv Funct Mater 2014;24:4823–30. doi:10.1002/adfm.201400647.
[9] Dmitriev RI, Borisov SM, Düssmann H, Sun S, Müller BJ, Prehn J, et al. Versatile Conjugated Polymer Nanoparticles for High-Resolution O2 Imaging in Cells and 3D Tissue Models. ACS Nano 2015;9:5275–88. doi:10.1021/acsnano.5b00771.
[10] Pu K, Shuhendler AJ, Rao J. Semiconducting Polymer Nanoprobe for In Vivo Imaging of Reactive Oxygen and Nitrogen Species. Angew Chem Int Ed 2013;52:10325–9. doi:10.1002/anie.201303420.
[11] Li P, Liu L, Xiao H, Zhang W, Wang L, Tang B. A New Polymer Nanoprobe Based on Chemiluminescence Resonance Energy Transfer for Ultrasensitive

Imaging of Intrinsic Superoxide Anion in Mice. J Am Chem Soc 2016;138:2893–6. doi:10.1021/jacs.5b11784.

[12] Frausto F, Thomas SW. Ratiometric Singlet Oxygen Detection in Water Using Acene-Doped Conjugated Polymer Nanoparticles. ACS Appl Mater Interfaces 2017;9:15768–75. doi:10.1021/acsami.7b02034.

[13] Chan Y-H, Wu C, Ye F, Jin Y, Smith PB, Chiu DT. Development of Ultrabright Semiconducting Polymer Dots for Ratiometric pH Sensing. Anal Chem 2011;83:1448–55. doi:10.1021/ac103140x.

[14] Ye F, Wu C, Jin Y, Chan Y-H, Zhang X, Chiu DT. Ratiometric Temperature Sensing with Semiconducting Polymer Dots. J Am Chem Soc 2011;133:8146–9. doi:10.1021/ja202945g.

[15] Huang Y-C, Chen C-P, Wu P-J, Kuo S-Y, Chan Y-H. Coumarin dye-embedded semiconducting polymer dots for ratiometric sensing of fluoride ions in aqueous solution and bio-imaging in cells. J Mater Chem B 2014;2:6188–91. doi:10.1039/C4TB01026D.

[16] Li S, Shen X, Li L, Yuan P, Guan Z, Yao SQ, et al. Conjugated-Polymer-Based Red-Emitting Nanoparticles for Two-Photon Excitation Cell Imaging with High Contrast. Langmuir 2014;30:7623–7. doi:10.1021/la501790y.

[17] Jiang Y, McNeill J. Light-Harvesting and Amplified Energy Transfer in Conjugated Polymer Nanoparticles. Chem Rev 2017;117:838–59. doi:10.1021/acs.chemrev.6b00419.

[18] Yuan H, Wang B, Lv F, Liu L, Wang S. Conjugated-Polymer-Based Energy-Transfer Systems for Antimicrobial and Anticancer Applications. Adv Mater 2014;26:6978–82. doi:10.1002/adma.201400379.

[19] Yu J, Rong Y, Kuo C-T, Zhou X-H, Chiu DT. Recent Advances in the Development of Highly Luminescent Semiconducting Polymer Dots and Nanoparticles for Biological Imaging and Medicine. Anal Chem 2017;89:42–56. doi:10.1021/acs.analchem.6b04672.

[20] Lyu Y, Pu K. Recent Advances of Activatable Molecular Probes Based on Semiconducting Polymer Nanoparticles in Sensing and Imaging. Adv Sci 2017;4:n/a-n/a. doi:10.1002/advs.201600481.

[21] Grimland JL, Wu C, Ramoutar RR, Brumaghim JL, McNeill J. Photosensitizer-doped conjugated polymer nanoparticles with high cross-sections for one- and two-photon excitation. Nanoscale 2011;3:1451–5. doi:10.1039/C0NR00834F.

[22] Bhattacharyya S, Barman MK, Baidya A, Patra A. Singlet Oxygen Generation from Polymer Nanoparticles–Photosensitizer Conjugates Using FRET Cascade. J Phys Chem C 2014;118:9733–40. doi:10.1021/jp4127094.

[23] He R, Hu M, Xu T, Li C, Wu C, Guo X, et al. Conjugated copolymer–photosensitizer molecular hybrids with broadband visible light absorption for efficient light-harvesting and enhanced singlet oxygen generation. J Mater Chem C 2015;3:973–6. doi:10.1039/C4TC02568G.

[24] Haimov E, Weitman H, Ickowicz D, Malik Z, Ehrenberg B. Pdots nanoparticles load photosensitizers and enhance efficiently their photodynamic effect by FRET. RSC Adv 2015;5:18482–91. doi:10.1039/C4RA15291C.

[25] Li S, Chang K, Sun K, Tang Y, Cui N, Wang Y, et al. Amplified Singlet Oxygen Generation in Semiconductor Polymer Dots for Photodynamic Cancer Therapy. ACS Appl Mater Interfaces 2016;8:3624–34. doi:10.1021/acsami.5b07995.

[26] Chang K, Tang Y, Fang X, Yin S, Xu H, Wu C. Incorporation of Porphyrin to π-Conjugated Backbone for Polymer-Dot-Sensitized Photodynamic Therapy. Biomacromolecules 2016;17:2128–36. doi:10.1021/acs.biomac.6b00356.

[27] Wu W, Feng G, Xu S, Liu B. A Photostable Far-Red/Near-Infrared Conjugated Polymer Photosensitizer with Aggregation-Induced Emission for Image-Guided Cancer Cell Ablation. Macromolecules 2016;49:5017–25. doi:10.1021/acs.macromol.6b00958.
[28] Shen X, Li L, Wu H, Yao SQ, Xu Q-H. Photosensitizer-doped conjugated polymer nanoparticles for simultaneous two-photon imaging and two-photon photodynamic therapy in living cells. Nanoscale 2011;3:5140–6. doi:10.1039/C1NR11104C.
[29] Tang Y, Chen H, Chang K, Liu Z, Wang Y, Qu S, et al. Photo-Cross-Linkable Polymer Dots with Stable Sensitizer Loading and Amplified Singlet Oxygen Generation for Photodynamic Therapy. ACS Appl Mater Interfaces 2017;9:3419–31. doi:10.1021/acsami.6b14325.
[30] Doshi M, Treglown K, Copik A, Gesquiere AJ. Composite Conjugated Polymer/Fullerene Nanoparticles as Sensitizers in Photodynamic Therapy for Cancer. BioNanoScience 2014;4:15–26. doi:10.1007/s12668-013-0114-5.
[31] Doshi M, Gesquiere AJ. Photodynamic Therapy with Blended Conducting Polymer/Fullerene Nanoparticle Photosensitizers. JoVE J Vis Exp 2015:e53038–e53038. doi:10.3791/53038.
[32] Banzo Jiménez AM. New insights in photodynamic theraphy: production, diffusion and reactivity of singlet oxygen in biological systems. Ph.D. Thesis. Universitat Ramon Llull, 2008.
[33] Wilkinson F, Brummer JG. Rate constants for the decay and reactions of the lowest electronically excited singlet state of molecular oxygen in solution. J Phys Chem Ref Data 1981;10:809–999. doi:10.1063/1.555655.
[34] Gandin E, Lion Y, Van de Vorst A. Quantum Yield of Singlet Oxygen Production by Xanthene Derivatives. Photochem Photobiol 1983;37:271–8. doi:10.1111/j.1751-1097.1983.tb04472.x.
[35] Omar Zahir K, Haim A. Yields of singlet dioxygen produced by the reaction between the excited state of tris(bipyridine)ruthenium(II) and triplet dioxygen in various solvents. J Photochem Photobiol Chem 1992;63:167–72. doi:10.1016/1010-6030(92)85132-E.
[36] Lindig BA, Rodgers MAJ, Schaap AP. Determination of the lifetime of singlet oxygen in water-d2 using 9,10-anthracenedipropionic acid, a water-soluble probe. J Am Chem Soc 1980;102:5590–3. doi:10.1021/ja00537a030.
[37] Schmidt R, Schaffner K, Trost W, Brauer HD. Wavelength-dependent and dual photochemistry of the endoperoxides of anthracene and 9,10-dimethylanthracene. J Phys Chem 1984;88:956–8. doi:10.1021/j150649a022.
[38] Haag WR, Hoigné J, Gassman E, Braun A. Singlet oxygen in surface waters — Part I: Furfuryl alcohol as a trapping agent. Chemosphere 1984;13:631–40. doi:10.1016/0045-6535(84)90199-1.
[39] Braun AM, Dahn H, Gassmann E, Gerothanassis I, Jakob L, Kateva J, et al. (2+4)-Cycloaddition with Singlet Oxygen. 17O-lnvestigation of the Reactivity of Furfuryl Alcohol Endoperoxide¶. Photochem Photobiol 1999;70:868–74. doi:10.1111/j.1751-1097.1999.tb08295.x.
[40] Chang Y-L, Palacios RE, Fan F-RF, Bard AJ, Barbara PF. Electrogenerated Chemiluminescence of Single Conjugated Polymer Nanoparticles. J Am Chem Soc 2008;130:8906–7. doi:10.1021/ja803454x.
[41] Palacios RE, Fan F-RF, Grey JK, Suk J, Bard AJ, Barbara PF. Charging and discharging of single conjugated-polymer nanoparticles. Nat Mater 2007;6:680–5. doi:10.1038/nmat1959.

[42] Szymanski C, Wu C, Hooper J, Salazar MA, Perdomo A, Dukes A, et al. Single molecule nanoparticles of the conjugated polymer MEH-PPV, preparation and characterization by near-field scanning optical microscopy. J Phys Chem B 2005;109:8543–8546.
[43] Arbeloa FL, Ojeda PR, Arbeloa IL. Flourescence self-quenching of the molecular forms of Rhodamine B in aqueous and ethanolic solutions. J Lumin 1989;44:105–12. doi:10.1016/0022-2313(89)90027-6.
[44] Bilski P, Dabestani R, Chignell CF. Influence of cationic surfactant on the photoprocesses of eosine and rose bengal in aqueous solution. J Phys Chem 1991;95:5784–91. doi:10.1021/j100168a015.
[45] Solis C, Torres JJ, Gsponer N, Previtali C, Palacios R, Montejano H, et al. Energy and electron transfer processes in polymeric nanoparticles. Photochem Photobiol Sci 2013;12:2146. doi:10.1039/c3pp50183c.
[46] Ponzio RA, Marcato YL, Gómez ML, Waiman CV, Chesta CA, Palacios RE. Crosslinked polymer nanoparticles containing single conjugated polymer chains. Methods Appl Fluoresc 2017;5:24001. doi:10.1088/2050-6120/aa6405.
[47] Nečas D, Klapetek P. Gwyddion: an open-source software for SPM data analysis. Open Phys 2012;10:181–8. doi:10.2478/s11534-011-0096-2.
[48] Watts B, Warnicke P, Pilet N, Raabe J. Nanoscale measurement of the absolute mass density of polymers: Nanoscale measurement of the absolute mass density of polymers. Phys Status Solidi A 2015;212:518–22. doi:10.1002/pssa.201400124.
[49] Baalousha M, Lead JR. Rationalizing Nanomaterial Sizes Measured by Atomic Force Microscopy, Flow Field-Flow Fractionation, and Dynamic Light Scattering: Sample Preparation, Polydispersity, and Particle Structure. Environ Sci Technol 2012;46:6134–42. doi:10.1021/es301167x.
[50] Groff LC, Wang X, McNeill JD. Measurement of Exciton Transport in Conjugated Polymer Nanoparticles. J Phys Chem C 2013;117:25748–55. doi:10.1021/jp407065h.
[51] Nifiatis F, Su W, Haley JE, Slagle JE, Cooper TM. Comparison of the Photophysical Properties of a Planar, PtOEP, and a Nonplanar, PtOETPP, Porphyrin in Solution and Doped Films. J Phys Chem A 2011;115:13764–72. doi:10.1021/jp205110j.
[52] Wu C, Zheng Y, Szymanski C, McNeill J. Energy Transfer in a Nanoscale Multichromophoric System: Fluorescent Dye-Doped Conjugated Polymer Nanoparticles. J Phys Chem C 2008;112:1772–81. doi:10.1021/jp074149+.
[53] Becker K, Lupton JM. Efficient Light Harvesting in Dye-Endcapped Conjugated Polymers Probed by Single Molecule Spectroscopy. J Am Chem Soc 2006;128:6468–79. doi:10.1021/ja0609405.
[54] Bansal AK, Holzer W, Penzkofer A, Tsuboi T. Absorption and emission spectroscopic characterization of platinum-octaethyl-porphyrin (PtOEP). Chem Phys 2006;330:118–29. doi:10.1016/j.chemphys.2006.08.002.
[55] Morgado J, Charas A, Fernandes JA, Gonçalves IS, Carlos LD, Alcácer L. Luminescence properties of composites made of a europium(III) complex and electroluminescent polymers with different energy gaps. J Phys Appl Phys 2006;39:3582–7. doi:10.1088/0022-3727/39/16/009.
[56] Baldo MA, Forrest SR. Transient analysis of organic electrophosphorescence: I. Transient analysis of triplet energy transfer. Phys Rev B 2000;62:10958–66. doi:10.1103/PhysRevB.62.10958.

[57] Gross EM, Armstrong NR, Wightman RM. Electrogenerated Chemiluminescence from Phosphorescent Molecules Used in Organic Light-Emitting Diodes. J Electrochem Soc 2002;149:E137–42. doi:10.1149/1.1464137.
[58] Fonseca SM, Pina J, Arnaut LG, Seixas de Melo J, Burrows HD, Chattopadhyay N, et al. Triplet-State and Singlet Oxygen Formation in Fluorene-Based Alternating Copolymers. J Phys Chem B 2006;110:8278–83. doi:10.1021/jp060251f.
[59] Bonneau R, Carmichael I, Hug GL. Molar absorption coefficients of transient species in solution. Pure Appl Chem 2009;63:289–300. doi:10.1351/pac199163020289.
[60] Aulin YV, Sebille M van, Moes M, Grozema FC. Photochemical upconversion in metal-based octaethyl porphyrin–diphenylanthracene systems. RSC Adv 2015;5:107896–903. doi:10.1039/C5RA20602B.
[61] Khan AU, Kasha M. Direct spectroscopic observation of singlet oxygen emission at 1268 nm excited by sensitizing dyes of biological interest in liquid solution. Proc Natl Acad Sci 1979;76:6047–9.
[62] Wilkinson F, Helman WP, Ross AB. Quantum Yields for the Photosensitized Formation of the Lowest Electronically Excited Singlet State of Molecular Oxygen in Solution. J Phys Chem Ref Data 1993;22:113–262. doi:10.1063/1.555934.
[63] Neckers DC. Rose Bengal. J Photochem Photobiol Chem 1989;47:1–29. doi:10.1016/1010-6030(89)85002-6.
[64] Merkel PB, Kearns DR. Radiationless decay of singlet molecular oxygen in solution. Experimental and theoretical study of electronic-to-vibrational energy transfer. J Am Chem Soc 1972;94:7244–53. doi:10.1021/ja00776a003.
[65] Rodgers MAJ. Solvent-induced deactivation of singlet oxygen: additivity relationships in nonaromatic solvents. J Am Chem Soc 1983;105:6201–5. doi:10.1021/ja00358a001.
[66] Dexter DL. A Theory of Sensitized Luminescence in Solids. J Chem Phys 1953;21:836–50. doi:10.1063/1.1699044.
[67] Maksimov MZ, Rozman IM. On the energy transfer in rigid solutions. Opt Spektrosk 1962;12:606–609.
[68] Lakowicz JR. Principles of Fluorescence Spectroscopy. 3rd ed. Springer; 2006.
[69] Yan L, Cui X, Harada T, Lincoln SF, Dai S, Kee TW. Generation of Fluorescent and Stable Conjugated Polymer Nanoparticles with Hydrophobically Modified Poly(acrylate)s. Macromolecules 2016;49:8530–9. doi:10.1021/acs.macromol.6b02002.
[70] Masel RI. Principles of Adsorption and Reaction on Solid Surfaces. 1 edition. New York: Wiley-Interscience; 1996.
[71] Su WP, Schrieffer JR, Heeger AJ. Solitons in Polyacetylene. Phys Rev Lett 1979;42:1698–701. doi:10.1103/PhysRevLett.42.1698.
[72] Heeger AJ, Kivelson S, Schrieffer JR, Su W-P. Solitons in conducting polymers. Rev Mod Phys 1988;60:781–850. doi:10.1103/RevModPhys.60.781.
[73] Schwartz BJ. Conjugated Polymers as molecular materials: How Chain Conformation and Film Morphology Influence Energy Transfer and Interchain Interactions. Annu Rev Phys Chem 2003;54:141–72. doi:10.1146/annurev.physchem.54.011002.103811.
[74] Yu J, Lammi R, Gesquiere AJ, Barbara PF. Singlet−Triplet and Triplet−Triplet Interactions in Conjugated Polymer Single Molecules. J Phys Chem B 2005;109:10025–34. doi:10.1021/jp0506742.

[75] Gesquiere AJ, Lee YJ, Yu J, Barbara PF. Single Molecule Modulation Spectroscopy of Conjugated Polymers. J Phys Chem B 2005;109:12366–71. doi:10.1021/jp0507851.
[76] Grey JK, Kim DY, Norris BC, Miller WL, Barbara PF. Size-Dependent Spectroscopic Properties of Conjugated Polymer Nanoparticles. J Phys Chem B 2006;110:25568–72. doi:10.1021/jp065990a.
[77] Palacios RE, Barbara PF. Single Molecule Spectroscopy of Poly 3-octyl-thiophene (P3OT). J Fluoresc 2007;17:749–57. doi:10.1007/s10895-007-0186-0.
[78] Barzykin AV, Tachiya M. Stochastic Model of Photodynamics in Multichromophoric Conjugated Polymers. J Phys Chem B 2006;110:7068–72. doi:10.1021/jp056088q.
[79] Lammi RK, Barbara PF. Influence of chain length on exciton migration to low-energy sites in single fluorene copolymers. Photochem Photobiol Sci 2005;4:95–9. doi:10.1039/B417753N.
[80] Gouterman M, Khalil G-E. Porphyrin free base phosphorescence. J Mol Spectrosc 1974;53:88–100. doi:10.1016/0022-2852(74)90263-X.
[81] Harriman A. Luminescence of porphyrins and metalloporphyrins. Part 1.—Zinc(II), nickel(II) and manganese(II) porphyrins. J Chem Soc Faraday Trans 1 Phys Chem Condens Phases 1980;76:1978–85. doi:10.1039/F19807601978.
[82] Völcker A, Adick H-J, Schmidt R, Brauer H-D. Near-infrared phosphorescence emission of compounds with low-lying triplet states. Chem Phys Lett 1989;159:103–8. doi:10.1016/S0009-2614(89)87462-7.